An Extended Virtual Aperture Imaging Model for Through-the-wall Sensing and Its Environmental Parameters Estimation

Yongping SONG, Tian JIN, Biying LU, Jun HU, Zhimin ZHOU

College of Electronics Science and Engineering, National University of Defense Technology, Changsha, 410073, China

sypopqjkl@163.com, tianjin@nudt.edu.cn

Abstract. *Through-the-wall imaging (TWI) radar has been given increasing attention in recent years. However, prior knowledge about environmental parameters, such as wall thickness and dielectric constant, and the standoff distance between an array and a wall, is generally unavailable in real applications. Thus, targets behind the wall suffer from defocusing and displacement under the conventional imaging operations. To solve this problem, in this paper, we first set up an extended imaging model of a virtual aperture obtained by a multiple-input-multiple-output array, which considers the array position to the wall and thus is more applicable for real situations. Then, we present a method to estimate the environmental parameters to calibrate the TWI, without multiple measurements or dominant scatterers behind-the-wall to assist. Simulation and field experiments were performed to illustrate the validity of the proposed imaging model and the environmental parameters estimation method.*

Keywords

Through-the-wall radar, environmental parameter estimation, virtual aperture, multiple-input multiple-output (MIMO).

1. Introduction

Through-the-wall sensing is highly desired in many civilian and military applications. Through-the-wall imaging radar (TWIR) achieves good wall penetration by transmitting low-frequency electromagnetic waves and provides imaging description of targets of interest behind walls [1-3] or the inside structure and layout of buildings [4-5]. Therefore, it has attracted more and more attention [6-10]. Generally speaking, two techniques, namely synthetic apertures and virtual apertures, are adopted in TWIR. Compared with the synthetic aperture formed by moving radar antennas, the virtual aperture obtained by the multiple-input multiple-output (MIMO) array can collect imaging data in a much shorter time and is thus more applicable for real-time implementation. In this paper, we focus on the MIMO array based TWIR.

When electromagnetic waves propagate in a layered medium composed of the air and wall, reflection and refraction will occur at the air-wall interface. This requires through-the-wall imaging (TWI) to consider the non-linear propagation path of electromagnetic waves, where some wall parameters, i.e., wall thickness and dielectric constant, are required to determine the propagation path. Currently, most through-the-wall image formations are based on the prior knowledge of the aforementioned wall parameters [11-13]. However, prior knowledge about these wall parameters is usually unavailable in practical applications, and the measured or estimated error of the wall parameters will greatly affect imaging quality of behind-the-wall targets [14]. Therefore, accurate estimation of wall parameters is an important technique in TWI.

The emerging techniques to estimate wall parameters can be categorized into three types. First, the image autofocusing method searches the reasonable wall parameters by assessing the image focusing quality [15]. It is effective but affords heavy computing burden. To improve the efficiency, an estimation method by minimizing the cross-range resolution of a special dominant scatterer rather than assessing the whole image was introduced in [16]. The method is invalid if there are no dominant scatterers behind the wall. Second, the wall parameters can be estimated by adjusting the array structure [17] or stand-off distance [18], both of which involve extra measurements. Third, echoes reflected by the wall are utilized to estimate the wall parameters. The dielectric constant can be provided by the back and forth propagation time if the wall thickness is known [19]. Moreover, searching the maximum of the correlation coefficient between the measured return and the corresponding estimating return in different wall parameters is also valid [20], and the greatest difficulty is the indecisive searching direction. Instead, using some special information extracted from echoes caused by the front surface and the rear surface of the wall is more promising, e.g., the dielectric constant can be estimated using the amplitude information of the front surface reflection [21]. Because the amplitude estimation is easily influenced by noise, a more practical method is presented by performing time-delay-only measurements in [22]; however, to achieve adequately high accuracy, it requires adjusting the transceiver-receiver separation repeatedly.

Furthermore, all of the above methods assume that the TWIR parallels the wall during data collection in the imaging model. When the array is placed close to the wall, the assumption can be easily met. However, in some applications, e.g., fire rescue, standoff operation is required. Therefore, it is necessary to setup a more reasonable model that considers the distance and inclination angle between the radar and wall. In such an extended imaging model for through-the-wall sensing, the unknown parameters include not only the traditional wall parameters, i.e., thickness and dielectric constant, but also the distance and the inclination angle. These four unknown parameters, denoted as the environmental parameters in this paper, are all required to be estimated in practical applications.

In the next section, an extended imaging model is proposed to fit the detection situation where a linear MIMO array sets in front of a wall with unknown distance and inclination angle. Then, in Section 3, we will show a novel environmental parameters estimation algorithm without any extra measurements or dominant scatters behind-the-wall to assist. To improve the image quality, an effective compensation imaging method for the proposed imaging model is introduced in Section 4. Section 5 & 6 show the corresponding processing results of the simulation and field measured data, which verify the imaging model and environmental parameters estimation algorithm. Conclusions will be drawn in Section 7.

2. Extend Virtual Aperture Imaging Model for TWI

The conventional linear MIMO array through-the-wall imaging model assumes an antenna array strictly parallel to the wall, as shown in Fig. 1. At this point, the relative position of the antenna array and the wall can be described with only one distance value R, which reduces complexity in image processing. However, in practice, limiting factors, such as the probe scene, make it difficult to ensure that the antenna array is strictly parallel to the wall, so it is necessary to extend the conventional model and take into consideration the case in which the wall inclines the antenna array.

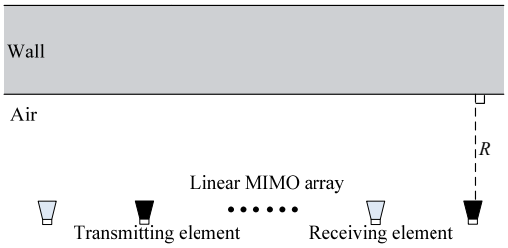

Fig. 1. Conventional linear MIMO array TWI model.

When the antenna array is inclined to the wall, the relative position of array and the wall needs to be described by both the distance and the inclination angle. For a linear MIMO array, the inclination angle can be described by one inclination angle θ. However, the array elements are at different distances to the wall. Because the array structure is known, we can consider anywhere in the array to be the reference position and use the reference position's distance to the wall to describe the distance information R from the array to the wall. Here we use the center of the array as the reference position.

Suppose we have a linear MIMO array TWIR with M transmitting elements and N receiving elements. To simplify our problem, we assume that the array is only inclined to the wall in the horizontal plane. Considering reflection and refraction caused by the wall, the imaging model can be expressed as Fig. 2.

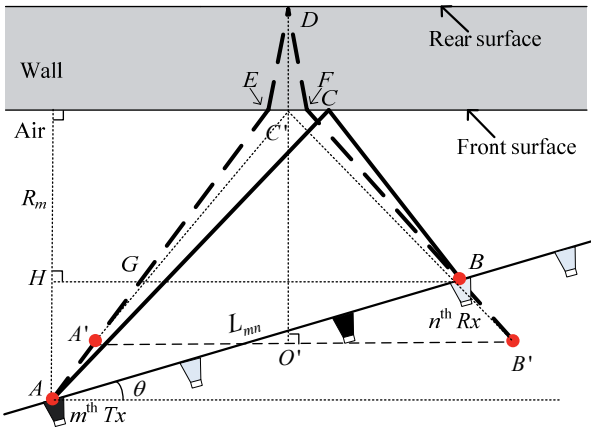

Fig. 2. TWI model of inclined linear MIMO array.

Fig. 2 shows a tilted linear MIMO array set in front of a wall with an inclination angle θ. When the left end point of the array is further from the wall than the right one, we define $\theta > 0$, otherwise $\theta < 0$. Obviously, $-90^\circ < \theta < 90^\circ$. Donate the m^{th} transmitting element as m^{th} Tx, and the n^{th} receiving element as n^{th} Rx. Then, the distance from m^{th} Tx to the wall is R_m.

Without consideration of the direct wave, the first two echoes are caused by the front surface and the rear surface of the wall, and the intersections of their propagation paths would be m^{th} Tx and n^{th} Rx. Donate A to be the location of m^{th} Tx, B to be the location of n^{th} Rx, and L_{mn} to be their spacing. C is the front surface echo reflection point, and the corresponding rear surface echo reflection point is D. Their respective refraction points are E and F. BH is parallel to the wall. G is the intersection of BH & AE. A' is the midpoint of AG. BB' is the extension line of FB, and $A'B' // BH$. $DO' \perp A'B'$, and C' is the intersection of DO' and the front surface.

It can be proved that for the echo propagation path of the front surface:

$$|AC| + |CB| = |A'C'| + |C'B'| \tag{1}$$

and for the echo propagation path of the rear surface:

$$|AE| + |ED| + |FD| + |BF| = |A'E| + |ED| + |FD| + |B'F| \tag{2}$$

Furthermore, the spacing of $A'B'$ is $L_{mn}\cos\theta$, and the

distance to the wall is $R_m + 0.5\alpha_{mn}L_{mn}\sin|\theta|$. When m^{th} *Tx* is further than n^{th} *Rx* from the wall, $\alpha_{mn} = -1$, otherwise $\alpha_{mn} = 1$ (See Appendix).

Thus, for the echo propagation paths of the front surface and the rear surface, the tilted linear MIMO array can be equivalent to several virtual element pairs whose connections are parallel to the wall.

3. Environmental Parameters Estimation of the Linear MIMO Array TWI Model

Already mentioned in the introduction, for our proposed linear MIMO array TWI model, the environmental parameters should include the distance of the array to the wall R , the inclination angle θ , the wall thickness d and the dielectric constant ε_r. We will use the conclusions in Section 2 to show the estimation method of the environmental parameters.

3.1 Estimation of *R* and θ

By the geometric relationship in Fig. 2 we get:

$$(ct_f(m,n))^2 - (L_{mn}\cos\theta)^2 = (2R_m + \alpha_{mn}L_{mn}\sin|\theta|)^2 \quad (3)$$

where, c is the light velocity in air, and $t_f(m,n)$ is the front surface echo delay caused by m^{th} *Tx* and n^{th} *Rx*. It can be further converted to:

$$c^2t_f^2(m,n) - L_{mn}^2 = 4R_m^2 + 4\alpha_{mn}L_{mn}R_m\sin|\theta| \quad (4)$$

set

$$g_{mn} = c^2t_f^2(m,n) - L_{mn}^2, \quad (5)$$

$$E_m = (R_m^2, R_m\sin|\theta|)^T, \quad (6)$$

$$h_{mn} = (4, 4\alpha_{mn}L_{mn}), \quad (7)$$

then

$$g_{mn} = h_{mn}E_m \quad (8)$$

Considering all the echoes generated by m^{th} *Tx*, we get

$$G_m = H_mE_m \quad (9)$$

where:

$$G_m = (g_{m1}, g_{m2}, \ldots, g_{mN})^T, \quad (10)$$

$$H_m = (h_{m1}^T, h_{m2}^T, \ldots, h_{mN}^T)^T. \quad (11)$$

Accordingly,

$$E_m = (H_m^TH_m)^{-1}H_m^TG_m. \quad (12)$$

That is, from

$$E_m = \begin{bmatrix} e_{m1} \\ e_{m2} \end{bmatrix} = \begin{bmatrix} R_m^2 \\ R_m\sin|\theta| \end{bmatrix} \quad (13)$$

we obtain the estimation of the distance R and the inclination angle θ on m^{th} *Tx*:

$$\begin{bmatrix} \hat{R}_m \\ |\hat{\theta}_m| \end{bmatrix} = \begin{bmatrix} \sqrt{e_{m1}} \\ \arcsin(e_{m2}/\sqrt{e_{m1}}) \end{bmatrix}. \quad (14)$$

By performing the same processing on the echo data of the remaining $M-1$ transmitting elements we will get

$$\hat{R}_E = (\hat{R}_1, \hat{R}_2, \ldots, \hat{R}_M)^T, \quad (15)$$

$$\hat{\theta}_E = (|\hat{\theta}_1|, |\hat{\theta}_2|, \ldots, |\hat{\theta}_M|)^T. \quad (16)$$

Taking the average of elements in vector $\hat{\theta}_E$ as the final estimation of $|\hat{\theta}|$:

$$|\hat{\theta}| = \frac{1}{M}\sum_{m=1}^{M}|\hat{\theta}_m|. \quad (17)$$

Then, if the left end point of the array is further from the wall than the right end point:

$$\hat{\theta} = -|\hat{\theta}|, \quad (18)$$

else

$$\hat{\theta} = |\hat{\theta}|. \quad (19)$$

Accordingly, $\hat{R}$, which represents the distance between the array and wall, can be estimated as:

$$\hat{R} = \sum_{m=1}^{M} w_m\hat{R}_m \quad (20)$$

wherein w_m is the weighting coefficient, which depends on the geometry of the antenna array.

3.2 Estimation of *d* and ε_r

It has been proved in Section 2 that m^{th} *Tx* and n^{th} *Rx* can be equivalent to a virtual element pair for the echo paths of the front surface and the rear surface. Denoting the virtual element pair as $m'n'$, with the estimation $\hat{R}_m$ and $\hat{\theta}$ in Section 3.1, the spacing of $m'n'$ can be expressed as:

$$\hat{L}_{m'n'} = L_{mn}\cos\hat{\theta} \quad (21)$$

and the distance of $m'n'$ to the wall $\hat{R}_{m'n'}$ is:

$$\hat{R}_{m'n'} = \hat{R}_m + 0.5\alpha_{mn}L_{mn}\sin|\hat{\theta}|. \quad (22)$$

So that the echo path model of the virtual element pair $m'n'$ can be showed as Fig. 3.

Because $m'n'$ is parallel to the wall, we have the following equation [23]:

$$d^2\varepsilon_r - \frac{d^2\hat{L}_{m'n'}^2\cos^2\hat{\theta}}{\hat{L}_{m'n'}^2\cos^2\hat{\theta} + 4\hat{R}_{m'n'}^2} = 0.25c^2t_d^2(m,n) \quad (23)$$

where

$$t_d(m,n) = t_r(m,n) - t_f(m,n). \quad (24)$$

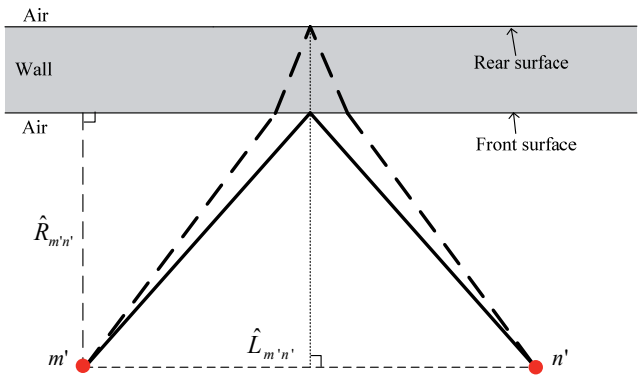

Fig. 3. The echo path model of a virtual element pair.

$t_r(m, n)$ is the rear surface echo delay caused by m^{th} *Tx* and n^{th} *Rx*. Then, we get:

$$Ap = b \tag{25}$$

where:

$$A = \begin{bmatrix} 1 & -\dfrac{\hat{L}_{1'1'}^2 \cos^2\hat{\theta}}{\hat{L}_{1'1'}^2 \cos^2\hat{\theta} + 4\hat{R}_{1'1'}^2} \\ 1 & -\dfrac{\hat{L}_{1'2'}^2 \cos^2\hat{\theta}}{\hat{L}_{1'2'}^2 \cos^2\hat{\theta} + 4\hat{R}_{1'2'}^2} \\ \vdots & \vdots \\ 1 & -\dfrac{\hat{L}_{M'N'}^2 \cos^2\hat{\theta}}{\hat{L}_{M'N'}^2 \cos^2\hat{\theta} + 4\hat{R}_{M'N'}^2} \end{bmatrix}_{MN\times 2} \tag{26}$$

$$p = \begin{bmatrix} d^2\varepsilon_r \\ d^2 \end{bmatrix}_{2\times 1} = \begin{bmatrix} p_1 \\ p_2 \end{bmatrix}_{2\times 1} \tag{27}$$

$$b = \begin{bmatrix} 0.25c^2 t_d^2(1,1) \\ 0.25c^2 t_d^2(1,2) \\ \vdots \\ 0.25c^2 t_d^2(M,N) \end{bmatrix}_{MN\times 1} \tag{28}$$

then:

$$p = (A^T A)^{-1} A^T b\,. \tag{29}$$

Finally, we can obtain the estimates of the left two environmental parameters:

$$\hat{d} = \sqrt{p_2}\,, \tag{30}$$

$$\hat{\varepsilon}_r = p_1 / p_2\,. \tag{31}$$

4. Compensation Image Formation Based on the Extended Virtual Aperture Imaging Model

Virtual aperture radar, such as MIMO radar using multi-elements, greatly improves detection performance. Accordingly, the imaging model becomes more complicated, which makes many traditional synthetic aperture radar imaging algorithms no longer applicable [24]. Due to the absence of any restrictions on the antenna array, the BP algorithm is widely used in virtual aperture radar imaging systems. We will use the environmental parameters estimated in Section 3 to show the compensation BP algorithm for the extended virtual aperture imaging model.

The BP algorithm replaces phase compensation by calculating the exact propagation delay of the target to the antenna elements [25]. In traditional through-the-wall BP imaging algorithm, the antenna array center is usually set as the origin, whereas the array itself is the abscissa. The direction perpendicular to the linear MIMO array is the ordinate. We name this coordinate system the antenna-coordinate-system. Correspondingly, the coordinate system that sets the front surface of the wall as the horizontal axis and the wall perpendicular as the longitudinal axis is called the wall-coordinate-system.

The purpose of TWI is usually to describe targets behind the wall. When the targets' position information is relative to the wall, interpretation of targets is easier. Therefore, using the wall-coordinate-system to show the results of TWI is more suitable. Assuming the array center is located in the center on the connection of m^{th} *Tx* and n^{th} *Rx*, we can obtain the TWI model in the wall-coordinate-system:

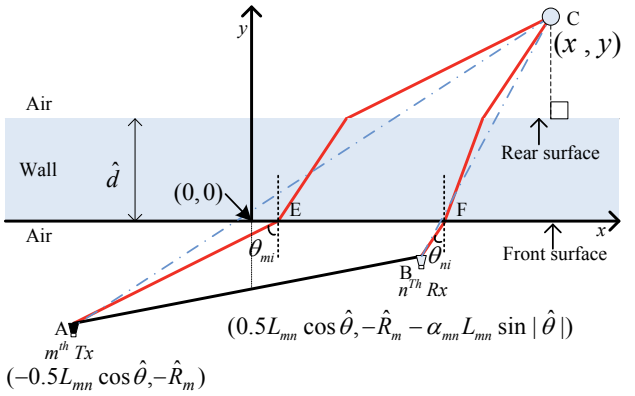

Fig. 4. TWI model in wall-coordinate-system.

According to the BP algorithm, the image value $I(x,y)$ of a point target (x,y) behind the wall could be calculated as follows:

$$I(x,y) = \sum_{m=1}^{M}\sum_{n=1}^{N} s_{mn}(t_{TE}(m,n)) \tag{32}$$

where, $s_{mn}(t_{TE}(m,n))$ represents the sampling at time $t_{TE}(m,n)$ in the echo generated by m^{th} *Tx* and n^{th} *Rx*. $t_{TE}(m,n)$ is the propagation delay from the point target to *mn*.

As shown in Fig. 4, $t_{TE}(m,n)$ can be obtained as:

$$t_{TE}(m,n) = \frac{l_{AC} + l_{BC}}{c} \tag{33}$$

l_{AC} is the propagation path from the target to m^{th} *Tx*, and l_{BC} is the propagation path from the target to n^{th} *Rx*.

The key to obtaining l_{AC} and l_{BC} is to determine the position of refraction points *E* and *F* in Fig. 4. Using the estimated thickness and dielectric constant of the wall, a quartic equation with one unknown quantity can be created to obtain the analytical solutions of the refraction point according to Snell's law [26] or to search for the location of refraction points by the minimum time criteria [27]. Both algorithms have high accuracy but costly calculations.

To avoid calculation resource depletion in solving the exact solutions, l_{AC} can be approximated by the expression [23]:

$$l_{AC} \approx r_{AC} + \hat{d}(\sqrt{\hat{\varepsilon}_r - \sin^2\theta_{mi}} - \cos\theta_{mi}) \tag{34}$$

where r_{AC} is the straight-line distance from the target to m^{th} *Tx*, and θ_{mi} is the incident angle of l_{AC}. θ_{mi} can be approximately obtained by:

$$\theta_{mi} \approx \arctan(\frac{x + 0.5L_{mn}\cos\hat{\theta}}{y + \hat{R}_m}). \tag{35}$$

Similarly:

$$l_{BC} \approx r_{BC} + \hat{d}(\sqrt{\hat{\varepsilon}_r - \sin^2\theta_{ni}} - \cos\theta_{ni}) \tag{36}$$

where r_{BC} is the straight-line distance from the target to n^{th} *Rx*, and θ_{ni} is the incident angle of l_{BC}.

In summary, for the point target (x, y) in the imaging scene, set:

$$\Delta r_m = \hat{d}(\sqrt{\hat{\varepsilon}_r - \sin^2\theta_{mi}} - \cos\theta_{mi}), \tag{37}$$

$$\Delta r_n = \hat{d}(\sqrt{\hat{\varepsilon}_r - \sin^2\theta_{ni}} - \cos\theta_{ni}), \tag{38}$$

then the propagation delay in the echo generated by m^{th} *Tx* and n^{th} *Rx* is calculated as follows:

$$t_{TE}(m,n) = \frac{r_{AC} + \beta\Delta r_m + r_{BC} + \beta\Delta r_n}{c} \tag{39}$$

where β is a scale factor to distinguish the positional relationship between the point target and the wall:

$$\beta = \begin{cases} 0 & , \quad y \le 0 \\ y/\hat{d} & , \quad 0 < y \le \hat{d} \\ 1 & , \quad y > \hat{d} \end{cases} \tag{40}$$

Combining formula (32), the pixel value on (*x,y*) can be obtained. By traversing every point in the imaging scene we can achieve the compensated image for the entire scene. Compared with conventional algorithms, the computation greatly reduces.

5. FDTD Simulations

Finite-difference-time-domain (FDTD) simulations are conducted to test the performance of our method. The MIMO array can be regarded as several associated single-input multiple-output (SIMO) arrays. To simplify the simulating complexity, a SIMO array is set in front of the wall:

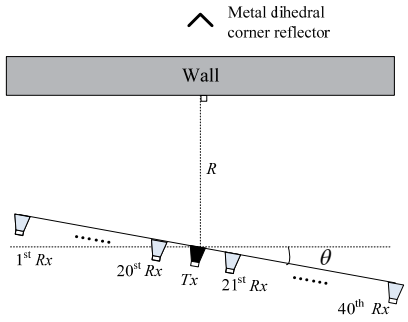

Fig. 5. The simulating scene.

It is excited by a Gaussian derivative pulse with 0.6 ns width. The white noise is added to the simulating echoes. The signal to noise ratio (SNR) is 15 dB. The estimation results are shown in Tab. 1 and Tab. 2.

$\theta(^\circ)$	$\hat{\theta}(^\circ)$	$\hat{R}$(m)	$\hat{d}$(m)	$\hat{\varepsilon}_r$
-5	-5.0708	1.4033	0.2002	4.2121
-10	-10.0998	1.4034	0.1936	4.5025
-15	-15.1011	1.4034	0.1915	4.6020
-25	-25.1440	1.4035	0.1875	4.7965
True value		1.4000	0.2000	4.5000

Tab. 1. Estimation results of the simulation data when R = 1.4 m.

R (m)	$\hat{R}$(m)	$\hat{\theta}(^\circ)$	$\hat{d}$(m)	$\hat{\varepsilon}_r$
1	1.0018	-15.1372	0.1994	4.2456
1.4	1.4034	-15.1011	0.1915	4.6020
1.8	1.8047	-15.0857	0.1944	4.4645
2.2	2.2058	-15.0642	0.1862	4.8620
True value		-15.0000	0.2000	4.5000

Tab. 2. Estimation results of the simulation data when $\theta = -15°$.

The results are satisfactory. To indicate the benefits of our virtual aperture imaging model, an imaging process is performed on the simulation data of R = 1.4 m and $\theta = -15°$:

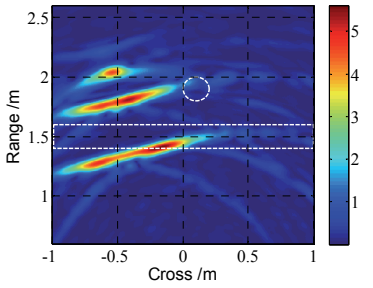

Fig. 6. BP imaging under the antenna-coordinate-system.

Without considering the array position to the wall, direct BP imaging has to be performed on the antenna-coordinate-system, resulting in whole scene bias. To make the scene easier to understand, the wall-coordinate-system should be built with the environment parameters $\hat{R}$ and $\hat{\theta}$:

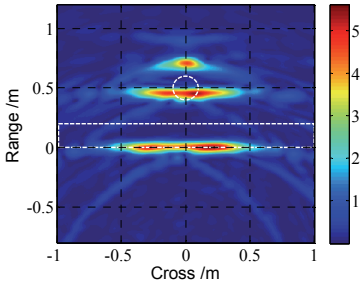

Fig. 7. BP imaging under the wall-coordinate-system.

Then, the defocusing and displacement of the target behind the wall can be fixed by the left two environment parameters $\hat{d}$ and $\hat{\varepsilon}_r$:

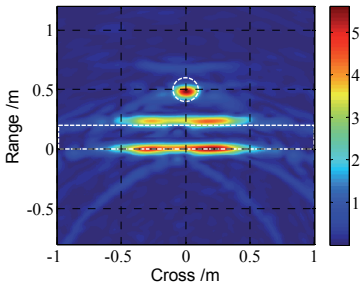

Fig. 8. BP imaging based on the extended virtual aperture imaging model.

Finally, benefiting from the extended virtual aperture imaging model, the quality of TWI is successfully enhanced.

6. Measurement Results

To validate the proposed imaging model and environmental parameter estimation algorithm, we have designed a vehicle virtual aperture radar system with 2 transmitting elements and 11 receiving elements. The transmitted signal is a stepping-frequency signal from 0.5 GHz to 3 GHz, and the step frequency is 2 MHz. The experiment scene and corresponding layout are shown in Fig. 9 and Fig. 10.

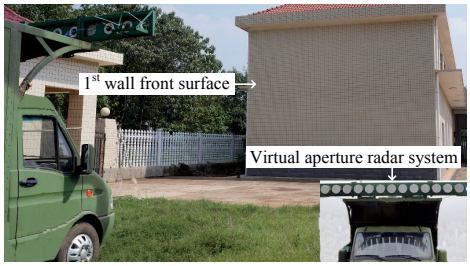

Fig. 9. The vehicle virtual aperture radar system and experiment scene.

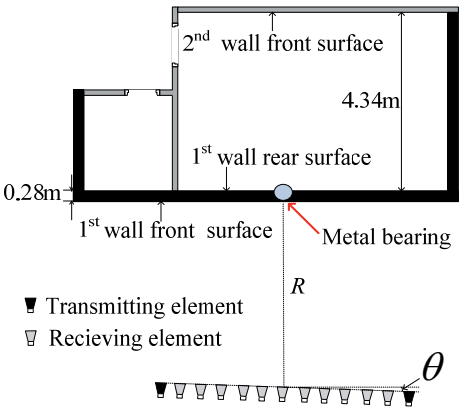

Fig. 10. Experiment layout.

The antenna array and the 1st wall are center-aligned. The distance from the array center to the wall is 11 m, and the measured inclination angle is –3.22°. The thickness of the 1st wall is 0.28 m, but the dielectric constant is unknown. In addition, there is a metal bearing in the center of the 1st wall, and we will see its shadowing effect in the later imaging result.

The derivation in Section 3 shows that the environmental parameters estimation depends on the echo time delay estimation of the front surface and rear surface. For the front surface echo, there are only reflections on the air-wall interface, so the dispersion effect is not serious. Therefore, by extracting the peak position of the echo processed by the matched-filter, we can obtain an effective echo time delay estimation of the front surface.

After the echo time delay estimation of the front surface is finished, we can obtain the relative position of the array and the 1st wall by $\hat{R}$ and $\hat{\theta}$. Using these two environmental parameters to build the wall-coordinate-system, we can achieve the BP imaging result without compensation, as shown in Fig. 11.

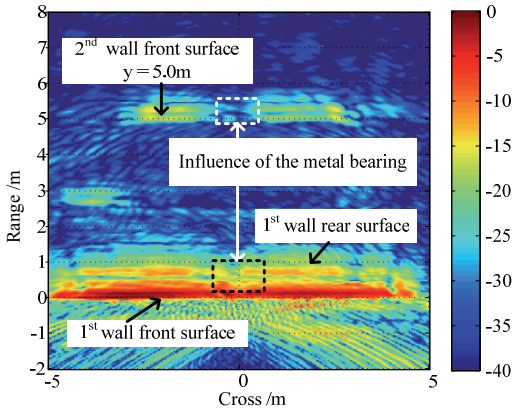

Fig. 11. BP imaging result without compensation under the wall-coordinate-system.

In Fig. 11, we obtain a relatively clear image of the building's inner structure. To show the proposed environmental parameters in this paper, we pay close attention to the 1st wall and the 2nd wall. By the shielding effect of the metal bearing, we find that the 1st wall rear surface and the

2nd wall have suffered different degrees of fault. Then, the range position of the 2nd wall front surface under the wall-coordinate-system should be 4.62 m from Fig. 6. However, it is approximately 5.0 m in Fig. 11. That is to say, the 2nd wall front surface lags 0.38 m because of the 1st wall. The 1st wall thickness is 0.28 m; thus, the deduced dielectric constant is 5.5561. This value can be used as a reference value to assess the final estimation result.

When estimating the echo time delay of the 1st wall rear surface, we have to consider the dispersion effect caused by the wall. Dispersion reduces the correlation between the echo and transmitting signal greatly, and this means that we cannot obtain an effective estimation of the 1st wall rear surface echo time delay from the traditional matched-filtering echo [28]. Protiva et al. proposed that the echo time-delay can be estimated by subspace decomposition on the deconvoluted echo data [29]. Based on this idea and referencing the frequency domain deconvolution methods, which are widely used in ultrasonic detection [30], we adopt the frequency domain Wiener inverse filter to complete deconvolution of the original echo data. Then, the maximum entropy (ME) power spectrum [31] is used to estimate the echo time delay of the 1st wall rear surface.

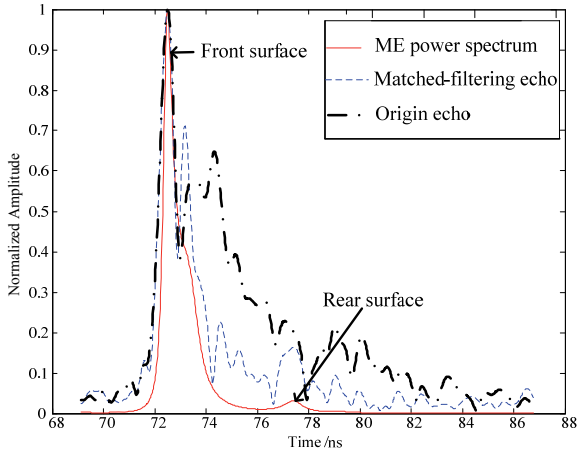

Fig. 12. Time delay estimation.

Fig. 12 shows the results of time delay estimation. With the help of deconvolution, the 1st wall rear surface echo becomes easy to identify in the ME power spectrum. Then, from Section 3.2, the wall thickness and dielectric constant can be estimated. The whole environmental estimation results are shown in Tab. 3.

	R (m)	θ (°)	d (m)	ε_r
Estimates	10.9256	-3.5409	0.2884	5.2273
True value	11.0000	-3.22	0.2800	5.5561
Relative error	-0.68%	9.97%	3.00%	-5.92%

Tab. 3. Estimation results of the environmental parameters.

Finally, we use these environmental parameters to obtain the compensation BP imaging for the echo data:

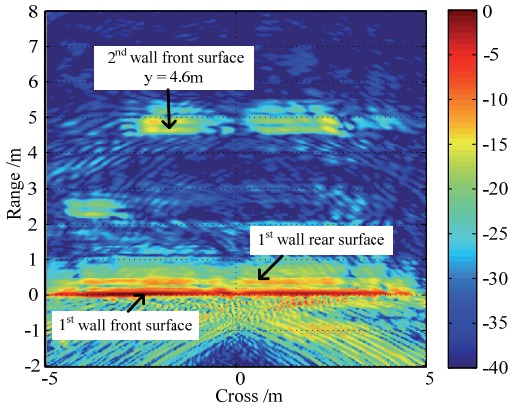

Fig. 13. Compensation BP imaging result.

The image entropy is commonly used to evaluate the image quality [32], and its definition is as follows:

$$H = \frac{(\sum_x \sum_y |I(x,y)|^2)^2}{\sum_x \sum_y |I(x,y)|^4}. \tag{41}$$

Usually, the smaller H is, the better the image quality is. Then, we use image entropy to evaluate the image with/without compensation, and the results are shown in Tab. 4.

	Image without compensation	Image with compensation
Image entropy	12161	9145

Tab. 4. The comparison of the image entropy in the image with/without compensation.

Combining Fig. 13 and Tab. 4, we find that by the compensation of environmental parameters, the position deviation of the scene behind the outer wall has been effectively corrected, and the image quality has also improved.

7. Conclusion

In this paper, an extended through-the-wall imaging model and its associated environmental parameters estimation algorithm are presented for the virtual aperture radar system. Because it has no special requirements for the array attitude, this imaging model is more suitable for the actual situation. Simultaneously, without any extra measurements or behind-the-wall dominant scatterers to assist, the environmental parameters estimation algorithm is of low computational complexity and easy to implement. The processing results of the measured data show the improvements to the through-the-wall imaging.

Furthermore, the environmental parameters estimation algorithm is tested on a single wall. In fact, it has the potential to estimate the parameters of multi walls, and this will be our future work.

Acknowledgements

This work is supported in part by the National Natural Science Foundation of China under Grant 61271441 and 61372161, and the research project of National University of Defense Technology under Grant CJ12-04-02.

Appendix

We mentioned in Section 2 that the element pair AB, which inclines the wall, can be equivalent to a virtual element pair $A'B'$, which parallels the wall. Here, we will prove this. Before proving, we reaffirm the relevant definitions and assumptions:

- m^{th} Tx is located at A, and its distance to the wall is R_m.
- n^{th} Rx is located at B, and the length of AB is L_{mn}.
- To simplify the proving process, we define that $\alpha_{mn} = -1$ when m^{th} Tx is further than n^{th} Rx from the wall. Otherwise, $\alpha_{mn} = 1$.

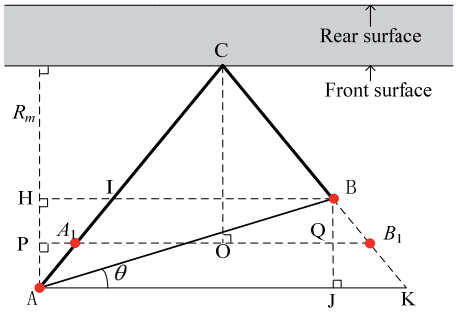

Fig. 14. The front surface echo path.

Fig. 14 shows the echo path of the front surface AK, and BH is parallel to the wall. K is the intersection of CB's extension line and AK. I is the intersection of BH and AC. P is the midpoint of AH, and B_1 is the midpoint of BK. $BJ \perp AK$. A_1 is the intersection of B_1P and AI, and Q is the intersection of B_1P and BJ. $CO \perp B_1P$.

$\because$ reflection law

$\therefore |AC| = |KC| \,\&\, |IC| = |BC|$

$\therefore |AI| = |KB|$

$\because P$ & B_1 are the midpoints of AH & BK, respectively.

$\therefore PB_1 \,//\, AK \,//\, BH$

$\therefore A_1$ & Q are the midpoints of AI & BJ, respectively.

$\therefore |AA_1| = |BB_1|$

Then, we have:

$$|AC| + |BC| = |A_1C| + |B_1C| \tag{42}$$

Therefore, AB is equivalent to A_1B_1 for the length of the rear surface echo path. Furthermore:

$$\Delta APA_1 \cong \Delta BQB_1 . \tag{43}$$

Then, for the isosceles ΔA_1CB_1

$$|A_1B_1| = |PQ| = L_{mn}\cos\theta , \tag{44}$$

$$|OC| = R_m + 0.5\alpha_{mn}L_{mn}\sin|\theta| . \tag{45}$$

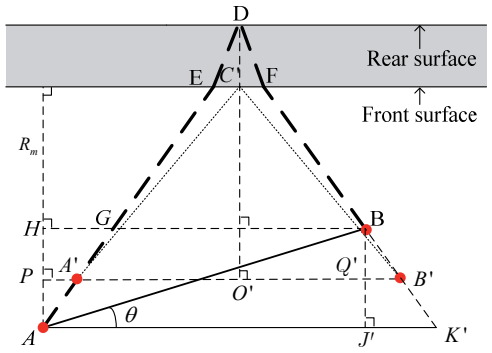

Fig. 15. The rear surface echo path.

Fig. 15 shows the echo path of the rear surface. AK' & BH are parallel to the wall. K' is the intersection of AK and the extension line of FB. G is the intersection of BH and AE. $BJ' \perp AK$, P& B' are the midpoints of AH & BK', respectively. A' is the intersection of $B'P$ and AG, and Q' is the intersection of $B'P$ and BJ'. D is the reflection point on the rear surface, $DO' \perp BH$, and C' is the intersection point of DO' and the front surface.

$\because$ reflection law & refraction law

$\therefore |AE| = |K'F| \,\&\, |GE| = |BF|$

$\therefore |AG| = |BK'|$

$\because P$ & B' are the midpoints of AH & BK', respectively.

$\therefore PB' \,//\, A'K \,//$ BH

$\therefore A'$ & Q' are the midpoints of AG & BJ', respectively.

$\therefore |AA'| = |BB'|$

Then, we have:

$$|AE| + |ED| + |FD| + |BF| = |A'E| + |ED| + |FD| + |B'F| \tag{46}$$

Therefore, AB is equivalent to $A'B'$ for the length of the rear surface echo path. Furthermore:

$$\Delta APA' \cong \Delta BQB' . \tag{47}$$

Then, for the isosceles $\Delta A'C'B'$:

$$|A'B'| = |PQ'| = L_{mn}\cos\theta , \tag{48}$$

$$|O'C'| = R_m + 0.5\alpha_{mn}L_{mn}\sin|\theta| . \tag{49}$$

According to (44) and (45), we get:

$$\Delta A'C'B' \cong \Delta A_1 C B_1 . \quad (50)$$

Consequently:

$$|AC| + |BC| = |A_1 C| + |B_1 C| = |A'C'| + |B'C'| . \quad (51)$$

So, AB is equivalent to $A'B'$ for the length of the front surface echo path.

In summary, for the path length of the echo from front and rear surface, m^{th} *Tx* and n^{th} *Rx*, whose connection AB inclines the wall, can be equivalent to a virtual element pair $A'B'$, which parallels the wall. The equivalent spacing is $L_{mn}\cos\theta$, and the equivalent distance to the wall is $R_m + 0.5\alpha_{mn}L_{mn}\sin|\theta|$ while $\alpha_{mn} = -1$ when m^{th} *Tx* is further than n^{th} *Rx* away from the wall. Otherwise, $\alpha_{mn} = 1$.

References

[1] CHETTY, K., SMITH, G. E., WOODBRIDGE, K. Through-the-wall sensing of personnel using passive bistatic wifi radar at standoff distances. *IEEE Transactions on Geoscience and Remote Sensing,* 2012, vol. 50, no. 4, p. 1218–1226.

[2] SU, Y. J. The research on receiver technology of the through-the-wall surveillance radar. *Journal of China Academy of Electronics and Information Technology,* 2011, vol. 6, no. 6, p. 648–651.

[3] LI, J., ZENG Z., SUN, J., LIU, F. Through-wall detection of human being's movement by UWB radar. *IEEE Geoscience and Remote Sensing Letters,* 2012, vol. 9, no. 6, p. 1079–1083.

[4] AFTANAS, M., DRUTAROVSKY, M. Imaging of the building contours with through the wall UWB radar system. *Radioengineering,* 2009, vol. 18, no. 3, p. 258–264.

[5] CHANG, P. C. Physics-based inverse processing and multi-path exploitation for through-wall radar imaging. *Doctor of Philosophy Thesis*. USA, Ohio State University, 2011.

[6] BARANOSKI, E. J. Through-wall imaging historical perspective and future directions. In *Proceedings of the IEEE International Conference on Acoustics, Speech and Signal Processing.* Las Vegas (USA), 2008, p. 5173–5176.

[7] SISMA, O., GAUGUE, A., LIEBE, CH., OGIER, J. M. UWB radar: vision through the wall. *Telecommun. Syst.,* 2008, vol. 38, no. 1 - 2, p. 53–59.

[8] SONG, L. P., YU, C., LIU, Q. H. Through wall imaging (TWI) by radar: 2-D tomo graphic results and analyses. *IEEE Transactions on Geoscience and Remote Sensing,* 2005, vol. 43, no. 12, p. 2793–2798.

[9] DEBES, C., AMIN, M. G., ZOUBIR, A. M. Target detection in single- and multiple-view through-the-wall radar imaging. *IEEE Transactions on Geoscience and Remote Sensing,* 2009, vol. 47, no. 5, p. 1349–1361.

[10] SHOUHEI, K., TAKUYA S., TORU, S. High resolution 3-D imaging algorithm with an envelope of modified spheres for UWB through-the-wall radars. *IEEE Transactions on Antennas and Propagation,* 2009, vol. 57, no. 11, p. 3520–3529.

[11] BROWNE, K. E., BURKHOLDER, R. J., VOLAKIS, J. L. Fast optimization of through-wall radar images via the method of Lagrange multipliers. *IEEE Transactions on Antennas and Propagation,* 2013, vol. 61, no. 1, p. 320–328.

[12] CHEN, P. H., NARAYANAN, R. M. Shifted pixel method for through-wall radar imaging. *IEEE Transactions on Antennas and Propagation,* 2012, vol. 60, no. 8, p. 3706–3716.

[13] WANG, Y., FATHY, A. E. Advanced system level simulation platform for three-dimensional UWB through-wall imaging SAR using time-domain approach. *IEEE Transactions on Geoscience and Remote Sensing,* 2012, vol. 50, no. 5, p. 1986–2000.

[14] LIU, X., LEUNG, H., LAMPROPOULOS, G. A. Effect of wall parameters on ultra-wideband synthetic aperture through-the-wall radar imaging. *IEEE Transactions on Aerospace and Electronic Systems,* 2012, vol. 48, no. 4, p. 3435–3449.

[15] LI, L., ZHANG, W., LI, F. A novel autofocusing approach for real-time through-wall imaging under unknown wall characteristics. *IEEE Transactions on Geoscience and Remote Sensing,* 2010, vol. 48, no. 1, p. 423–431.

[16] JIN, T., CHEN, B., ZHOU, Z. Image-domain estimation of wall parameters for autofocusing of through-the-wall SAR imagery. *IEEE Transactions on Geoscience and Remote Sensing*, 2013, vol. 51, no. 3, p. 1836–1843.

[17] WANG, G. Y., AMIN, M. G. ZHANG, Y. M. New approach for target locations in the presence of wall ambiguities. *IEEE Transactions on Aerospace and Electronic System,* 2006, vol. 42, no. 1, p. 301–315.

[18] WANG, G. Y., AMIN, M. G. Imaging through unknown walls using different standoff distances. *IEEE Transactions on Signal Processing,* 2006, vol. 54, no. 10, p. 4015–4025.

[19] SAGNARD, F., ZEIN, G. E. In situ characterization of building materials for propagation modeling: frequency and time responses. *IEEE Transactions on Antennas and Propagation*, 2005, vol. 53, no. 10, p. 3166–3173.

[20] LI, X., HUANG, X., JIN, T. Estimation of wall parameters by exploiting correlation of echoes in time domain. *Electronics Letters*, 2010, vol. 46, no. 23, p. 1563–1564.

[21] AFTANAS, M., SACHS, J., DRUTAROVSKY, M., KOCUR, D. Efficient and fast method of wall parameter estimation by using UWB radar system. *Frequenz Journal*, 2009, vol. 63, no. 11 - 12, p. 231–235.

[22] PROTIVA, P., MRKVICA, J., MACHAC, J. Estimation of wall parameters from time-delay-only through-wall radar measurements. *IEEE Transactions on Antennas and Propagation,* 2011, vol. 59, no. 11, p. 4268–4278.

[23] JIN, T., CHEN, B., ZHOU, Z. Estimation of wall parameters for cognitive imaging in through-the-wall radar. In *Proceedings of the 2012 IEEE 11th International Conference on Signal Processing.* Beijing (China), 2012, p. 1936–1939.

[24] MCCORKLE, J. W. Focusing of synthetic aperture ultra wideband data. In *Proceedings of the IEEE International Conference on Systems Engineering.* Dayton (USA), 1991, p. 1–5.

[25] WANG, H. J., HUANG, C. L., LU, M., SU, Y. Back projection imaging algorithm for MIMO radar. *Systems Engineering and Electronics (China),* 2010, vol. 32, no. 8, p. 1567 - 1673.

[26] AHMAD, F., AMIN, M. G., KASSAM, S. A. Synthetic aperture beamformer for imaging through a dielectric wall. *IEEE Transactions on Aerospace and Electronic Systems,* 2005, vol. 41, no. 1, p. 271–283.

[27] JIA, Y., KONG, L., YANG, X. Improved cross-correlated back-projection algorithm for through-wall-radar imaging. In *Proceedings of the 2013 IEEE Radar Conference.* Ottawa (Canada), 2013, p. 1–3.

[28] WEISS, L. G. Wavelets and wideband correlation processing. *IEEE Signal Processing Magazine,* 1994, vol. 11, no. 1, p. 13–32.

[29] PROTIVA, P., MRKVICA, J., MACHAC, J. Time delay estimation of UWB radar signals backscattered from a wall. *Microwave & Optical Technology Lett.,* 2011, vol. 53, no. 6, p. 1444 to 1450.

[30] ALI, M. G. S., ELSAYED, N. Z., EBEID, M. R. Signal processing of ultrasonic data by frequency domain deconvolution. *Walailak*

Journal of Science and Technology, 2013, vol. 10, no. 3, p. 297 to 304.

[31] QIU, T. S., WANG, H. Y. A high time delay estimation based on the maximum entropy power spectrum estimation. *Journal of Electronics (China),* 1997, vol. 14, no. 3, p. 279–284.

[32] LI, L., ZHANG, W., LI, F. A novel autofocusing approach for real-time through-wall imaging under unknown wall characteristics. *IEEE Transactions on Geoscience and Remote Sensing,* 2010, vol. 48, no. 1, p. 423–431.

About Authors ...

YONGPING SONG received his B.S. degree in Electronic Engineering from the National University of Defense Technology, Changsha, China in 2012, and now he is studying for the M.S. degree in Information and Communication Engineering. His research interests include radar imaging and automatic target detection.

TIAN JIN received B.S., M.S. and Ph.D. degrees in Information and Communication Engineering from the National University of Defense Technology, Changsha, China, in 2002, 2003, and 2007, respectively. He is currently an associate professor of the National University of Defense Technology. His Ph.D. dissertation was awarded as the National Excellent Doctoral dissertation of China in 2009. His fields of interest include radar imaging, automatic target detection, and machine learning.